Journal of Sound and Vibration 333 (2014) 4376–4401

Contents lists available at ScienceDirect

Journal of Sound and Vibration

journal homepage: www.elsevier.com/locate/jsvi

Numerical and experimental analysis of uncertainty on modal parameters estimated with the stochastic subspace method

Gilles Tondreau*, Arnaud Deraemaeker

ULB, Building Architecture and Town Planning, 50 av. Franklin Roosevelt, CP 194/02, B-1050 Brussels, Belgium

ARTICLE INFO

Article history:
Received 9 October 2013
Received in revised form
15 April 2014
Accepted 18 April 2014
Handling Editor: K. Shin
Available online 13 May 2014

ABSTRACT

Modal parameters of structures are often used as inputs for finite element model updating, vibration control, structural design or structural health monitoring (SHM). In order to test the robustness of these methods, it is a common practice to introduce uncertainty on the eigenfrequencies and modal damping coefficients under the form of a Gaussian perturbation, while the uncertainty on the mode shapes is modeled in the form of independent Gaussian noise at each measured location. A more rigorous approach consists however in adding uncorrelated noise on the time domain responses at each sensor before proceeding to an operational modal analysis. In this paper, we study in detail the resulting uncertainty when modal analysis is performed using the stochastic subspace identification method. A Monte-Carlo simulation is performed on a simply supported beam, and the uncertainty on a set of 5000 modal parameters identified with the stochastic subspace identification method is discussed. Next, 4000 experimental modal identifications of a small clamped–free steel plate equipped with 8 piezoelectric patches are performed in order to confirm the conclusions drawn in the numerical case study. In particular, the results point out that the uncertainty on eigenfrequencies and modal damping coefficients may exhibit a non-normal distribution, and that there is a non-negligible spatial correlation between the uncertainty on mode shapes at sensors of different locations.

1. Introduction

Further to huge advances in the development of operational modal analysis (OMA) tools [1,2], there is an increasing interest in the estimation of modal parameters from vibration responses for different purposes. Finite element model updating which consists in adapting a numerical model of the structure of interest is a field in which modal parameters are extensively used. Typically, finite element model updating aims at improving the numerical models by minimizing the distance between the measured data and the model by modifying the numerical model. While any dynamic signature can be considered for this purpose (time histories, frequency responses or energies for instance), the use of mode shapes and eigenfrequencies is probably the most common approach [3–5].

Methods considering modal parameters for damage assessment have been widely studied in the last few decades. The techniques for structural health monitoring (SHM) can be classified into two big families, depending on the need or not of a numerical physical model (finite element model) of the structure of interest. Doebling et al. propose a detailed overview of

* Corresponding author.
E-mail addresses: gilles.tondreau@ulb.ac.be (G. Tondreau), aderaema@ulb.ac.be (A. Deraemaeker).

http://dx.doi.org/10.1016/j.jsv.2014.04.039
0022-460X/

the first category of methods based on updating modal parameters in [6]. While model-based methods require a numerical model of the structure to identify the damage, the second category of methods which is referred to as data-based methods rely only on measured data to identify damage. While time domain responses of sensors can be used for damage assessment by considering guided waves [7], or autoregressive models [8–10], methods using frequency responses and modal parameters are much more studied. The use of eigenfrequencies has been widely investigated for damage assessment, since cracks typically decreases the eigenfrequencies. Salawu provides a wide overview of the methods using changes of eigenfrequencies for damage assessment in [11]. Modal damping coefficients have also been considered for structural health monitoring: cracks create new surfaces increasing the dissipation energy in most cases [12], but these parameters are more sensitive to the test procedure as well as to the analysis methods than eigenfrequencies, making them less reliable [13]. While eigenfrequencies and modal damping coefficients are global structural parameters, mode shapes are locally affected by a damage, which makes them particularly interesting to locate the damages. The most straightforward way to proceed consists in comparing directly the undamaged and the damaged mode shapes. The idea to locate damage from curvature mode shapes has been proposed by Pandey in [14], since it has been observed that the effect of damage is located in the close vicinity of the damage. Other methods use approximations of the stiffness and flexibility matrices [15] from the identified mode shapes and eigenfrequencies in order to locate damages. Stubbs and Kim have also proposed in [16] to take advantage of the decrease of strain modal energy in beam-like structures to identify the position of damages, and the technique has been extended to plate-like structures in [17].

Because noise is always present in measurements, and that operational modal analysis introduces some uncertainty in the identified modal parameters [18], the validation of the previous methods calls for a study of their efficiency when some uncertainty is taken into account in the modal parameters of interest. Traditionally, when testing the robustness of such types of methods, numerical models are used in order to compute the modal parameters which will be used as input measurements, and noise is added directly on the modal parameters. Most of the time, robustness studies consider uncertainties on the mode shapes in the form of independent white noise added at each measured location such as in [19–21]. Similarly, the uncertainty on the identified eigenfrequencies and modal damping coefficients consist very often in perturbing the reference eigenfrequency or modal damping with a white noise (Gaussian noise), as in [22]. Other research studies consider noise added directly on the time domain sensor response which is more realistic, but the methods developed are mainly using time domain sensor responses, as in [23,24].

Several studies which deal with the estimation of the uncertainty on modal parameters from a single stochastic subspace identification can be found in the literature [18,25,26]. Using a perturbation analysis, these techniques are interesting to estimate the variance of identified eigenfrequencies and modal damping coefficients as well as the covariance of the identified mode shapes, and are usually validated with a Monte-Carlo simulation which is much more computationally expensive, but which gives a better estimation of the (co)variances. However, Carden and Mita pointed out in [27] that the modal parameters may exhibit non-normal distribution, and that the variances are not adequate to estimate the confidence intervals in that case. The aim of the present paper is to study in detail the effect of noise measurement on the uncertainty of modal parameters obtained with stochastic subspace identification [1]. A Monte-Carlo simulation on a numerical case study and an experimental validation are performed. These results are used to assess the uncertainty on the modal parameters obtained with successive modal identifications, and a comparison is performed when the uncertainty is directly added on the modal parameters obtained with a unique modal identification.

This paper is organized as follows: Section 2 deals with a numerical study of the uncertainty on modal parameters due to measurement noise. The structure investigated is a simply supported beam equipped with 11 equally distributed strain sensors. 5000 samples of the dynamic response of the beam excited by a band-limited white noise signal are computed, and the modal properties are identified for each sample. Noise measurement is added directly on the sensor responses before the modal identification, and we compare the uncertainty obtained on eigenfrequencies, modal damping coefficients and mode shapes with the classic approach in which the uncertainty is modeled as a Gaussian noise added directly on the modal parameters. In particular, the correlation matrices are computed for each mode shape of interest and show that the classic approach for which the noise of the mode shapes projected on the sensors is added independently at each sensor location neglects the spatial correlation which exists between the noise of sensors at different locations. Section 3 investigates the experimental uncertainty of modal parameters on a small clamped–free steel plate equipped with 8 piezoelectric patches and excited with piezoceramic patch. The same analysis as in the numerical case study is performed, and the experimental results confirm the main numerical observations which are: (i) the spatial correlation in the noise of mode shapes between sensors at different locations, and (ii) the non-normal distribution of the identified eigenfrequencies and modal damping coefficients. These observations illustrate very well that the robustness with respect to noise measurement of any method using modal parameters should be based on Monte-Carlo simulations in which the noise is introduced on the sensor responses in time domain, before the modal identification.

2. Numerical study of the uncertainty on modal parameters due to measurement noise

2.1. Description of the case study

The numerical case study deals with a 1 m × 0.1 m × 0.1 m simply supported beam made of concrete (Fig. 1) that has already been investigated [28]. The beam is modeled with 100 Euler–Bernoulli beam elements using the *Structural Dynamics*

Fig. 1. Simply supported concrete beam equipped with 11 strain sensors.

Toolbox under *Matlab* [29], and a force with a band-limited white noise between 0 Hz and 4000 Hz exciting the first four modes (at 193 Hz, 773 Hz, 1740 Hz and 3094 Hz) is applied. A network of 11 equally spaced strain sensors with a gauge length of 0.01 m is placed on the beam, and their time histories are obtained thanks to an in-house numerical simulator which is applying a time integration scheme based on Duhamel's formula [30], and which has already been used in [31]. Each measurement lasts for 10 s with a sampling rate of 8000 Hz, resulting in a set of 80 000 measurement points for each sensor. The noise added on the sensor responses takes the following form:

$$y_n(t) = y_n^0(t) + \underbrace{\beta_1 \lambda \max_{[0\ s,10\ s]} (y_n^0(t))}_{\text{noise}}, \tag{1}$$

where $y_n(t)$ and $y_n^0(t)$ are the noisy and non-noisy responses of sensor n ($n = 1, \ldots, 11$) at time t respectively. λ is the random parameter, with its continuous distribution $f(\lambda)$ following a Gaussian distribution with zero mean and unitary standard deviation as it is usually assumed [32], and will be confirmed experimentally in Sections 3.2 and 3.3. The level of noise β_1 is fixed at 5 percent, which leads to a signal-to-noise ratio (SNR) around 25 for each sensor, when SNR is defined as the ratio between the average power of the signal y_n and the average power of the corresponding noise during the 10 s of measurements:

$$\text{SNR} = \frac{P_{y_n}}{P_{\text{noise}}} = \left(\frac{\text{RMS}(y_n)}{\text{RMS}(\text{noise})} \right)^2, \tag{2}$$

where RMS stands for the root mean square. The modal identification is performed using the covariance based stochastic subspace identification method (SSI-cov) [18] implemented in the *Macec Toolbox* [2] under *Matlab*, using output-only measurements.

The modal identification is performed 5000 times with different realizations of the input excitation signal and the output measurement noise on the sensors. After a brief description of the stochastic subspace identification method, the following sections will study the effect of noise on the uncertainty of the modal parameters that will be obtained using that operational modal analysis technique.

2.2. Operational modal analysis based on the stochastic subspace identification method

Before discussing the uncertainty on modal parameters estimated with the stochastic subspace method, we briefly present this output-only technique which is the most commonly used for operational modal analysis.

The discrete-time state-space model of a mechanical structure reads as

$$\begin{aligned} \mathbf{x_{k+1}} &= \mathbf{A x_k} + \mathbf{B f_k} \\ \mathbf{y_k} &= \mathbf{C x_k} + \mathbf{D f_k} + \mathbf{n_{y,k}} \end{aligned} \tag{3}$$

where $\mathbf{x_k}$ is the state of the structure, $\mathbf{y_k}$ the outputs (measured), and $\mathbf{n_{y,k}}$ the output measurement noise. A zero-order hold assumption is made on the (not measured) inputs $\mathbf{f_k}$. The stochastic terms

$$\begin{aligned} \mathbf{w_k} &= \mathbf{B f_k} \\ \mathbf{v_k} &= \mathbf{D f_k} + \mathbf{n_{y,k}} \end{aligned} \tag{4}$$

are unknown but assumed to have a discrete white noise nature with an expected value equal to zero [18]. The concept of subspace identification for linear systems applied to modal analysis of structures [33] uses the Hankel matrix. In the case of the covariance based stochastic subspace identification method applied in this study, the Hankel matrix reads as [34]

$$\mathbf{H_{p,q}} = \begin{bmatrix} \Lambda_0 & \Lambda_1 & \cdots & \cdots & \Lambda_{q-1} \\ \Lambda_1 & \Lambda_2 & \cdots & \cdots & \Lambda_q \\ \vdots & \vdots & \cdots & \cdots & \vdots \\ \Lambda_{p-1} & \Lambda_p & \cdots & \cdots & \Lambda_{p+q-2} \end{bmatrix}, \tag{5}$$

where the parameters p and q are chosen by the user so that $p \geq q$. Each component Λ_i of the Hankel matrix represents the output covariance matrix estimated from a set of N samples y_k:

$$\Lambda_i = \frac{1}{N-i} \sum_{k=1}^{N-i} y_{k+i} y_k^T \tag{6}$$

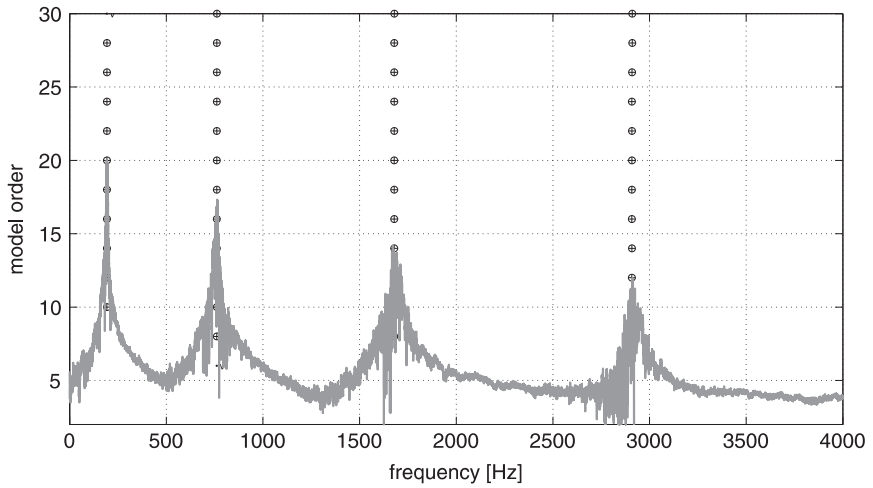

Fig. 2. Stabilization diagram obtained with one sample of the numerical case study (the grey thick curve represents the sum of PSDs of all sensors).

This Hankel matrix can be factorized into two subspaces from which the modal information can be extracted. The **A** and **C** matrices of the discrete-time state-space model (Eq. (3)) can be extracted from the Hankel matrix. The mode shapes, eigenfrequencies and damping ratios can finally be identified from these matrices.

2.3. Uncertainty on mode shapes

Fig. 2 shows the stabilization diagram from which the modal parameters have been automatically identified. In the present case study, the default model order for all mode shapes has been fixed to 16. However, such a choice of model order failed in the automated modal identification of several samples, so that it has been necessary to manually identify the modal parameters with other model orders between 10 and 15.

The first four bending mode shapes have been identified after each of the N measurement and each realization is noted as $\boldsymbol{\Phi}_{i,k}$ ($k=1,\ldots,5000$ and $i=1$, 2, 3 or 4). The ith reference mode shape $\boldsymbol{\Phi}_i^0$ is the mean of the $N=5000$ identified mode shapes:

$$\boldsymbol{\Phi}_i^0 = \frac{1}{N}\sum_{k=1}^{N} \boldsymbol{\Phi}_{i,k}, \tag{7}$$

with $\boldsymbol{\Phi}_{i,k} = \{\phi_{i,k1} \cdots \phi_{i,k11}\}^T$. Note that the SSI-cov method implemented in *Macec* normalizes the mode shapes with respect to the largest component, which leads to a zero covariance for that component. The modes are therefore renormalized using their Euclidian norm: $\tilde{\boldsymbol{\Phi}}_{i,k} = \boldsymbol{\Phi}_{i,k}/\|\boldsymbol{\Phi}_{i,k}\|$. Since all the modes considered in this paper will be normalized based on their Euclidian norm, we will use the notation $\boldsymbol{\Phi}_{i,k}$ instead of $\tilde{\boldsymbol{\Phi}}_{i,k}$ in the rest of the paper in order to simplify notations. A very simple manner to introduce noise on mode shapes which has been adopted in several studies is to add spatially uncorrelated noise directly on the mode shapes:

$$\phi_{i,kn} = \phi_{i,n}^0 + \beta_2 \lambda \phi_{i,n}^0, \tag{8}$$

where $\phi_{i,kn}$ is the nth component of the kth noisy sample of mode i, and $\phi_{i,n}^0$ is the corresponding non-noisy component. Similar to Eq. (1), β_2 is the level of noise and λ follows a normal distribution $f(\lambda)$ with zero mean and unitary standard deviation.

Because the effect on mode shapes of a noise introduced following Eq. (1) or (8) is very different, we cannot choose $\beta_1 = \beta_2$ if we wish to have noise on mode shapes that are of the same order of magnitude. In particular, the level of noise in Equation (1) depends on the position of the excitation while the one in Eq. (8) is only related to the mode shape, so that there is no way to link β_1 with β_2. We have therefore arbitrarily fixed the value of β_2 using the mean value of noise on all sensors as follows:

$$\beta_2 = \frac{1}{11}\sum_{n=1}^{11} \beta_1 \max_{[0\ s,10\ s]} (y_n^0(t)), \tag{9}$$

which leads to $\beta_2 = 0.858$ percent. For clarity, we will refer to the solutions obtained with Eqs. (1) and (8) as schemes S_1 and S_2 respectively.

Before the statistical analysis on the identified mode shapes, it has been chosen to proceed to a first cleaning of the obtained mode shapes in order to remove the mode shapes which have been badly identified. One mode automatically identified is rejected if the MAC value (modal assurance criterion, [35]) computed between the current mode shape $\boldsymbol{\Phi}_{i,k}$ and

the reference mode shape $\boldsymbol{\Phi}_i^0$ is smaller than 0.9:

$$\mathrm{MAC}(\boldsymbol{\Phi}_{i,k}, \boldsymbol{\Phi}_i^0) = \frac{\boldsymbol{\Phi}_{i,k}^T \boldsymbol{\Phi}_i^0}{(\boldsymbol{\Phi}_{i,k}^T \boldsymbol{\Phi}_{i,k})(\boldsymbol{\Phi}_i^{0T} \boldsymbol{\Phi}_i^0)} < 0.9 \tag{10}$$

As it can be seen from Table 1, only a very few modal identifications failed. In order to quantify the spatial correlation between the uncertainty on the different mode shape components, we compute the correlation matrices as defined in [36] of the identified mode shapes for modes 1, 2, 3 and 4 separately. If we note $\mathbf{C}_i$ the correlation matrix of mode shape $\boldsymbol{\Phi}_i$ based on n_s samples, the spatial correlation between sensors m and n reads as

$$c_{i,mn} = \frac{\sum_{k=1}^{n_s} (\phi_{i,km} - \phi_{i,m}^0)(\phi_{i,kn} - \phi_{i,n}^0)}{(n_s - 1)\sigma_m \sigma_n}, \tag{11}$$

where σ_m and σ_n are the estimated standard deviations of sensors m and n. Before analyzing the spatial correlation between the sensors, it was necessary to check that the correlation matrices taken into account can be considered as converged. In order to do that, we have computed the evolution of the normalized modal difference (NMD) [35] for each column of the correlation matrix $\mathbf{C}_i$ (for scheme S_1), as a function of the number of samples:

$$\mathrm{NMD}(\mathbf{C}_{i,n_s}, \mathbf{C}_{i,n_s-50}) = \sqrt{\frac{1 - \mathrm{MAC}(\mathbf{C}_{i,n_s}, \mathbf{C}_{i,n_s-50})}{\mathrm{MAC}(\mathbf{C}_{i,n_s}, \mathbf{C}_{i,n_s-50})}}, \tag{12}$$

where the MAC is computed between a specific column of the correlation matrix computed with n_s samples ($\mathbf{C}_{i,n_s}$) and the same column of the correlation matrix computed with $n_s - 50$ samples ($\mathbf{C}_{i,n_s-50}$). Fig. 3 depicts the evolution of NMD for the first column of the covariance matrix $\mathbf{C}_1$ for the four mode shapes of interest.

From that plot, we can conclude that the estimate of the correlation matrix can be considered as converged when we take into account all the N samples summarized in Table 1, since the NMD value is below 1 percent from 3000 samples for all the mode shapes. The same conclusion can be made by analyzing the evolution of NMD computed for the other columns of the correlation matrix.

In addition to this preliminary test, another verification has been made to guarantee that the variability described by the covariance matrices was mainly due to the noise acting on the sensors, and not due to the identification process itself. The idea that has been applied consisted in performing 5000 identifications without noise added on the sensors (with different realizations of the input signal), and to compute the resulting covariance matrix. This matrix was found to be several orders of magnitude lower than the covariance matrix computed with noise added on the sensors.

Fig. 4 shows the mean of the identified mode shapes, as well as the 10σ intervals. In particular, it has been observed that the distribution of each mode shape component was very close to a normal distribution centered on the mean value of the modal component, as depicted in Fig. 5 for the fifth sensor of the first mode shape. In this figure, we also provide the normal

Table 1
Success rates of modal identifications.

Success quantifier	$\boldsymbol{\Phi}_1$	$\boldsymbol{\Phi}_2$	$\boldsymbol{\Phi}_3$	$\boldsymbol{\Phi}_4$
Number of samples retained N	4998	4999	4998	5000
Proportion of failed identifications (%)	0.04	0.02	0.04	0

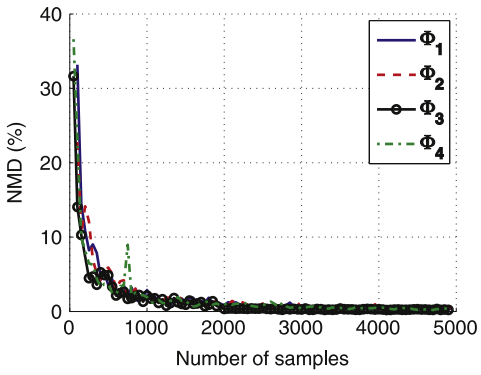

Fig. 3. Evolution of NMD with the number of samples (first column of the correlation matrix $\mathbf{C}_1$).

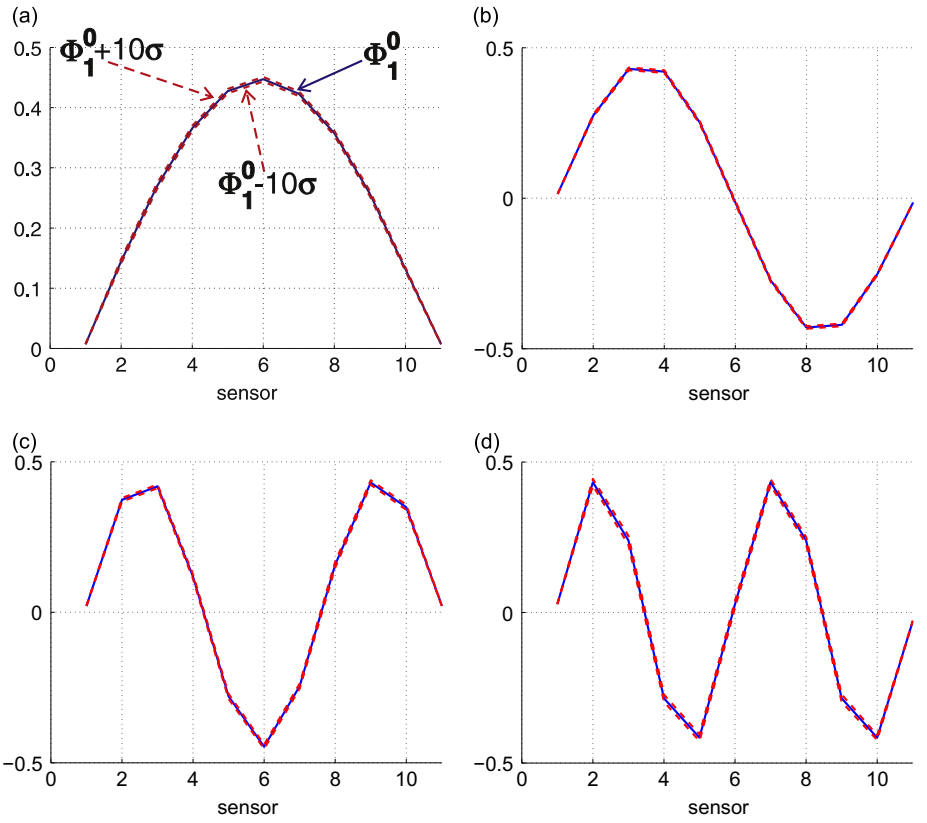

Fig. 4. Uncertainty on the first four identified mode shapes (scheme S_1). Full line: mode shape (mean over all samples), dashed line: 10σ interval. (a) $\boldsymbol{\Phi}_1$, (b) $\boldsymbol{\Phi}_2$, (c) $\boldsymbol{\Phi}_3$, (d) $\boldsymbol{\Phi}_4$.

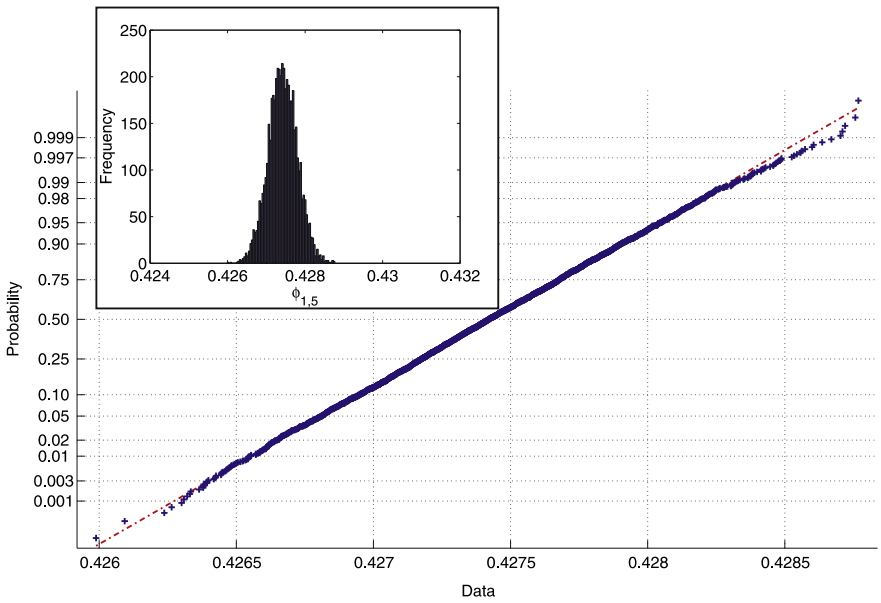

Fig. 5. Normal probability plot and histogram for the fifth component of $\boldsymbol{\Phi}_1$. Dashed line: normal distribution, crosses: sample data.

probability plot which is a graphical tool often used in statistics in order to check the normality of a random variable [37]. In this plot, the samples of the random variable of interest are ranked from smallest to largest, and plotted against their cumulative frequency. If the normal distribution describes correctly the random variable, the plotted points will follow closely a straight line.

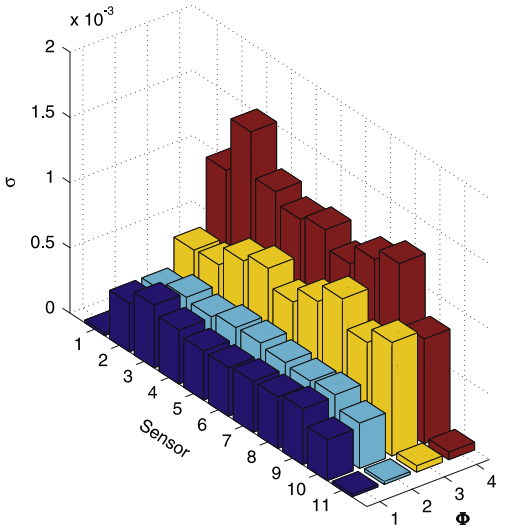

Fig. 6. Variance on the identified mode shape components (scheme S_1).

Fig. 6 shows that for the present numerical case study, the uncertainty σ on the modal components increases when modes of increasing order are identified.

It is interesting to compare the two noise schemes previously defined by considering the correlation matrices. Indeed, because noise is added independently on each component of the mode shape with scheme S_2, the correlation matrix of $\boldsymbol{\Phi}_i$ will converge to a diagonal matrix. On the other hand, the correlation matrix for scheme S_1 is clearly not diagonal, showing that the noises on each component are not independent. Fig. 7 plots the correlation coefficients obtained with noise modeling scheme S_1 for the third sensor (third column/row of the correlation matrix).

Scheme S_2 presents columns close to unitary vectors because the noise is added independently on each component as already explained. The noise at sensor m has therefore no influence on the other sensors $m \neq n$. On the other hand, with scheme S_1, noise at sensor m influences the noise at the other sensors. Note that a non-negligible correlation can exist between distant sensors such as sensors 3 and 9 (Fig. 7(d)). We have also checked that there is no correlation between two different mode shapes. Indeed, if we define the spatial correlation between sensors m and n for mode shapes i and j as follows:

$$c_{ij,mn} = \frac{\sum_{k=1}^{n_s} (\phi_{i,km} - \phi_{i,m}^0)(\phi_{j,kn} - \phi_{j,n}^0)}{(n_s - 1)\sigma_{im}\sigma_{jn}}, \tag{13}$$

we found that $c_{ij,mn}$ was very close to 0 for all mode shapes $m \neq n$ and all sensors.

By performing a singular value decomposition of the correlation matrix based on Eq. (11), it is possible to represent the variability in the form of uncorrelated variables. Because $\mathbf{C}_i$ is symmetric, the singular value decomposition reads as

$$\mathbf{C}_i = \mathbf{U}_i \mathbf{S}_i \mathbf{U}_i^T \tag{14}$$

Whatever the noise scheme considered, each noisy normalized mode shape can be decomposed into its noisy and non-noisy parts as $\boldsymbol{\Phi}_{i,k} = \boldsymbol{\Phi}_i^0 + \delta\boldsymbol{\Phi}_{i,k}$, where the noisy part of sample k can be rebuilt by combining the eigenvectors of $\mathbf{U}_i$:

$$\delta\boldsymbol{\Phi}_{i,k} = \mathbf{U}_i \boldsymbol{\alpha}_k^T \tag{15}$$

Fig. 8 shows the different energy distributions of the two noise schemes. Scheme S_1 has a spatial correlation which is explained by 10 principal components with decreasing energy, amongst which one or two components have a clear predominant contribution (Fig. 8(a), (c) and (d)). On the other hand, scheme S_2 shows an almost constant energy distribution on all the 11 components. Comparing the eigenvectors $\mathbf{u}_j$ of $\mathbf{U}_i$ allows us to figure out how the energy is distributed in an uncorrelated variables space (Fig. 9).

Since the correlation matrix of scheme S_2 is the identity matrix by definition of this uncorrelated noise modeling, the eigenvectors are pulses because the noise is already described in an independent variables space. On the other hand, the eigenvectors corresponding to the noise scheme S_1 are waves of different lengths due to the spatial correlation. We can therefore conclude that the models based on scheme S_2 generally adopted to introduce some uncertainty on the identification of the mode shapes are not very realistic. By considering Eq. (15), we see that the noise on mode shapes can be computed thanks to a linear combination of eigenvectors, of which linear coefficients $\boldsymbol{\alpha}_k = \{\alpha_{1,k} \cdots \alpha_{11,k}\}$ are random variables. It is therefore interesting to study the statistical distribution of these coefficients. In the case of noise scheme S_1,

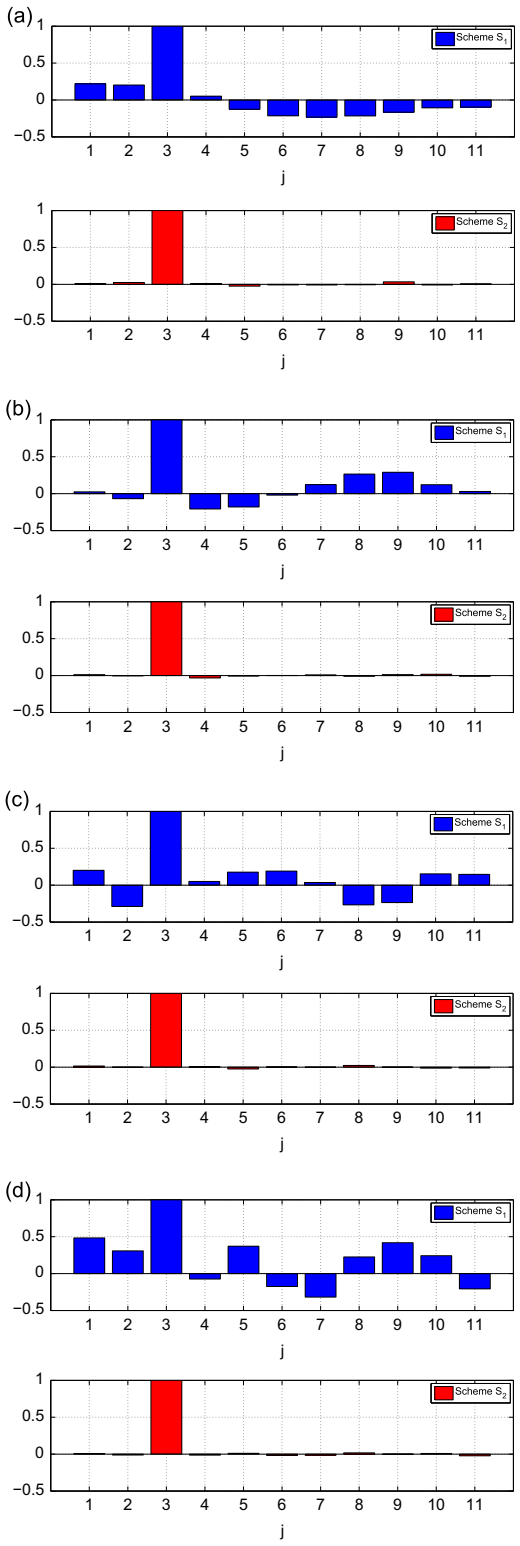

Fig. 7. Correlation coefficients for sensor 3. (a) $\mathbf{\Phi}_1$, (b) $\mathbf{\Phi}_2$, (c) $\mathbf{\Phi}_3$, (d) $\mathbf{\Phi}_4$.

the coefficients $\alpha_{n,k}$ $(n=1,\ldots,11)$ have been found to be approximatively normally distributed, as it can be seen in Fig. 10 which shows the statistical distribution of the coefficient $\alpha_{2,k}$ corresponding to the first sensor of $\delta\mathbf{\Phi}_{2,k}$ (noise on the first sensor for the second mode shape).

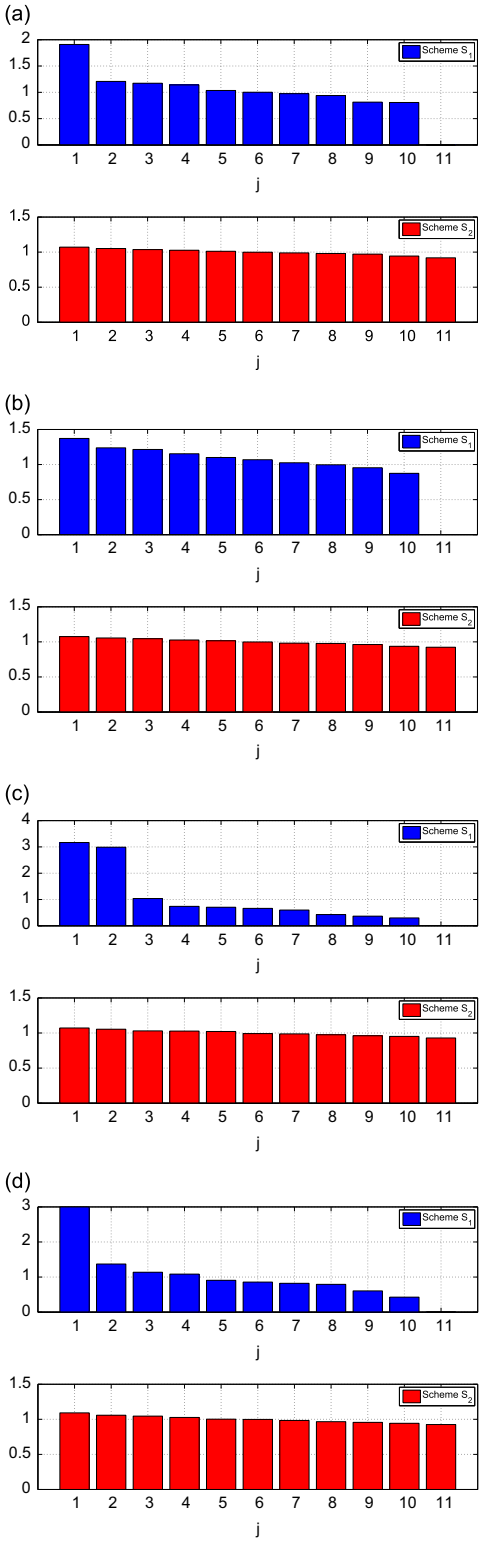

Fig. 8. Comparison of the singular values for schemes S_1 and S_2. (a) $\mathbf{\Phi}_1$, (b) $\mathbf{\Phi}_2$, (c) $\mathbf{\Phi}_3$, (d) $\mathbf{\Phi}_4$.

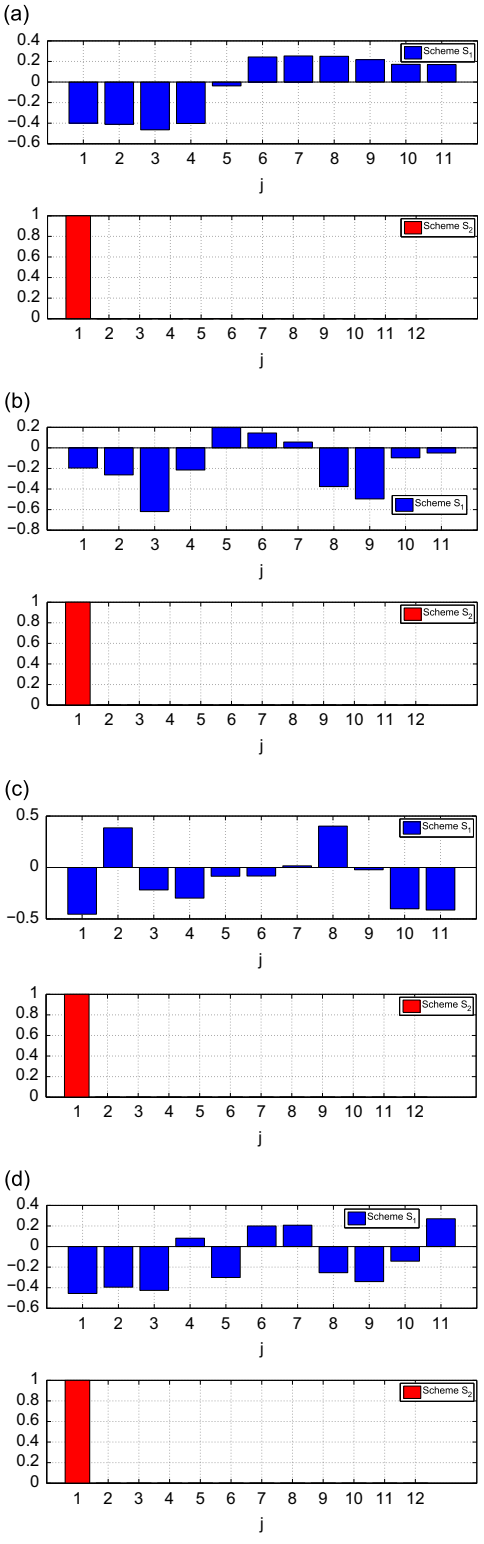

Fig. 9. Comparison of the first eigenvector for schemes S_1 and S_2. (a) $\mathbf{\Phi}_1$, (b) $\mathbf{\Phi}_2$, (c) $\mathbf{\Phi}_3$, (d) $\mathbf{\Phi}_4$.

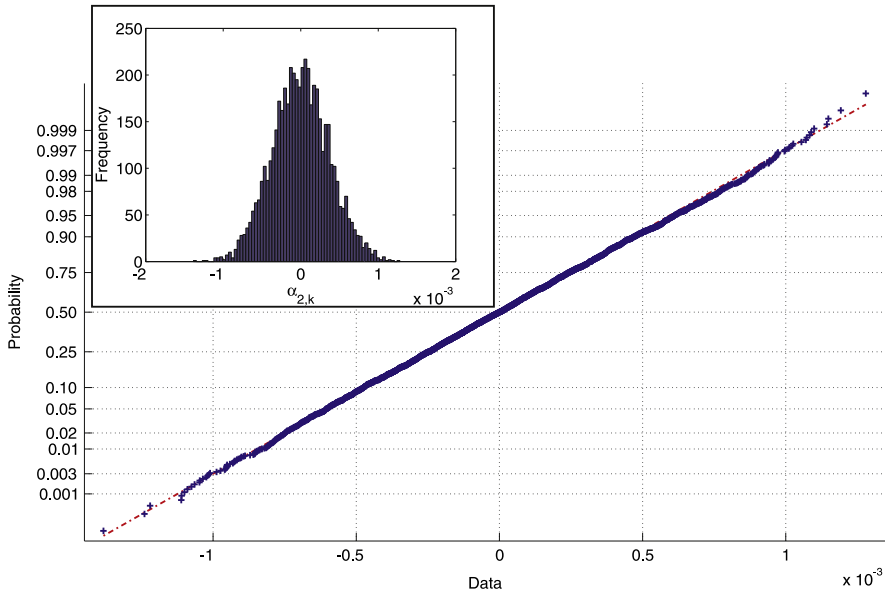

Fig. 10. Normal probability plot and histogram for $\alpha_{2,k}$ (sensor 1). Dashed line: normal distribution, crosses: sample data.

Table 2
Uncertainties on the identified eigenfrequencies.

	μ (Hz)	σ (%)
f_1	192.56	0.0792
f_2	760.99	0.0115
f_3	1679.1	0.0130
f_4	2908.2	0.0136

The same analysis for the noise scheme S_2 leads also to coefficients $\alpha_{i,k}$ as normally distributed, due to the definition of that noise scheme.

2.4. Uncertainty on eigenfrequencies and modal damping coefficients

This section investigates the uncertainty due to the noise measurement on the eigenfrequencies and the modal damping coefficients of the first four mode shapes. Tables 2 and 3 summarize the mean values and the corresponding standard deviations of each eigenfrequency and modal damping coefficient.

These two tables illustrate very well the fact that the eigenfrequencies can be identified with a high accuracy, while it is more difficult to identify the modal damping coefficients, since they present a much higher standard deviation. A common practice which is widely applied in the literature consists in adding an uncorrelated white noise independently on each modal parameter, as suggested below:

$$\theta_i = \theta_i^0 + \beta\lambda\theta_i^0, \tag{16}$$

where θ_i is the ith noisy eigenfrequency or modal damping coefficient and θ_i^0 the corresponding non-noisy value. Similar to the noise scheme S_1, λ is a random parameter, with its continuous distribution $f(\lambda)$ following a Gaussian distribution with zero mean and unitary standard deviation. For this reason, it is interesting to check the correlation of uncertainties on the modal parameters, as well as their normality. From Fig. 11, it seems that the hypothesis of uncorrelated noise is acceptable, since the correlation matrices of f_i and ξ_i are mostly diagonal.

The normal probability plots of Fig. 12 show that the assumption of a normal distribution is a quite rough approximation. Indeed, despite the fact that the noise acting on the sensors is Gaussian, the uncertainty on the eigenfrequencies and modal damping coefficients obtained with a stochastic subspace identification method is not Gaussian: the data in the tails of the normal probability plot clearly departs from the straight line, which is an indication that the normal distribution is not a good model for the eigenfrequency and the modal damping.

Table 3
Uncertainties on the identified modal damping coefficients.

	μ (%)	σ (%)
ξ_1	1.0004	0.0596
ξ_2	1.0000	0.0131
ξ_3	1.0034	0.1791
ξ_4	1.0010	0.0762

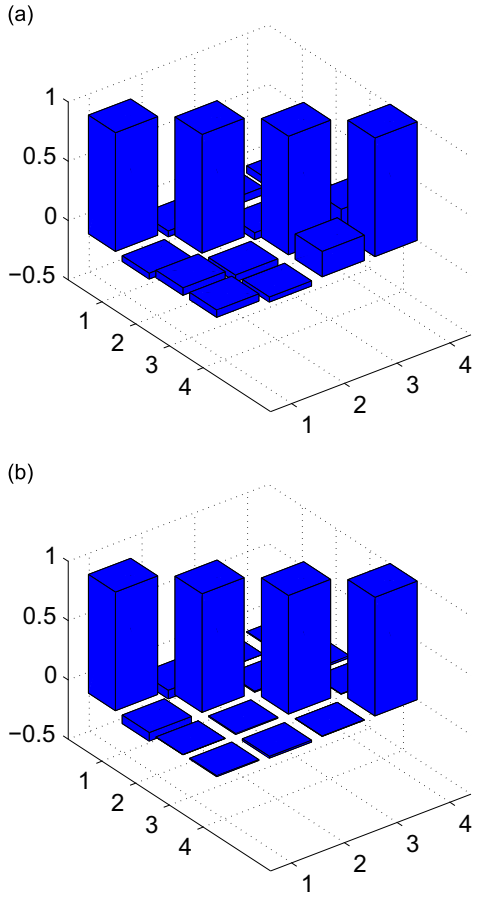

Fig. 11. Correlation of the uncertainty on the (a) eigenfrequencies and (b) modal damping coefficients.

3. Experimental study of the uncertainty on modal parameters due to measurement noise

In order to confirm the observations that have been obtained in the previous numerical study, it has been decided to develop a small experimental setup in order to assess the effect of real noise measurement on the uncertainty of the identification of modal parameters. The present section summarizes the experimental results. As with the numerical investigation, we analyze first the uncertainty on mode shapes with a particular emphasis on the spatial correlation between the sensors, and then analyze the uncertainty on the eigenfrequencies and the modal damping coefficients.

3.1. Description of the case study

The structure consists in a 100 mm × 670 mm × 3 mm clamped–free steel plate as shown in Fig. 13, and was studied in [38] in the context of experimental damage localization. One PZT actuator is used to excite the structure, and eight 13 mm × 60 mm × 50 μmm low-cost PVDFs sensors have been fixed with double-coated tape. These sensors which measure the average dynamic strains over the area where they are glued are numbered from the clamped edge of the plate, and cover continuously the structure along its length. A National Instrument PXIe-1082 data acquisition system with a NI PXIe-4492

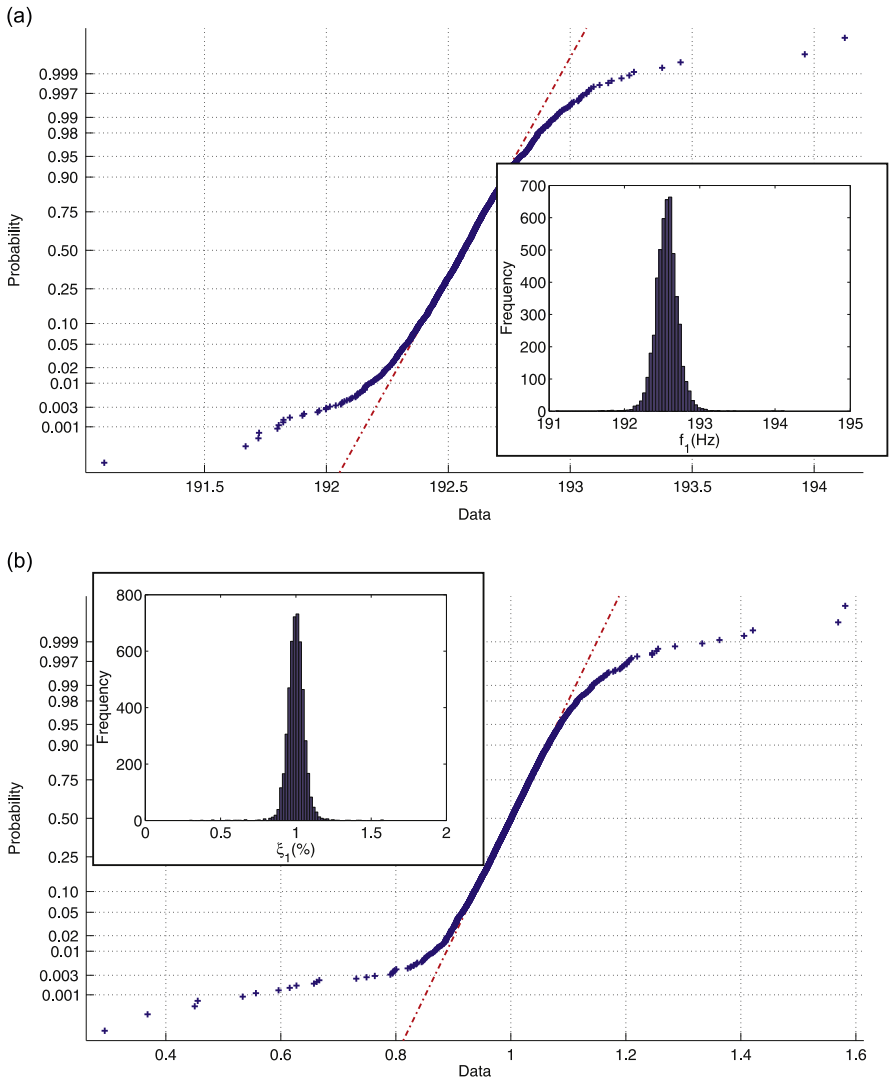

Fig. 12. Normal probability plots and histograms of the eigenfrequencies and modal damping coefficients corresponding to the first mode shape. Dashed line: normal distribution, crosses: sample data. (a) f_1, (b) ξ_1.

module (24 bits) is used to measure the eight voltages from the PVDFs at the same time. The PZT actuator is driven with a band-limited white noise between 0 Hz and 50 Hz generated by the PXI, and powered by a MIDE high voltage amplifier.

3.2. *Verification of noise of the acquisition system*

We have first performed measurements without any sensor connected to the NI PXIe-4492 module, in order to study the noise of the acquisition system itself. This study aims at characterizing the noise of the different channels, and to check if there is any form of correlation between them. For this purpose, we measure the empty channels for different sampling frequencies, as well as different levels of full-scale range (± 1 V and ± 10 V). In order to be statistically comparable, the different tests consider the same number of measurement points (102 400), leading to different durations of acquisitions T for each sampling frequency f_s, which are summarized in Table 4.

Fig. 14 displays the evolution of the level of noise (variance σ of the time histories) with respect to the sampling frequency for the different channels.

We observe two general properties which are already known [32]: the noise increases with (i) the full-scale range and (ii) with the sampling frequency. We have also checked that the channel presenting the maximum level of noise changes arbitrarily with the sampling frequency.

As it can be seen in Fig. 15, the noise is uncorrelated and follows a normal distribution on all the channels.

Moreover, the noise between the channels is normally distributed, which can justify the uncorrelated white noise scheme S_1 on the sensors proposed in Section 2 (Eq. (1)).

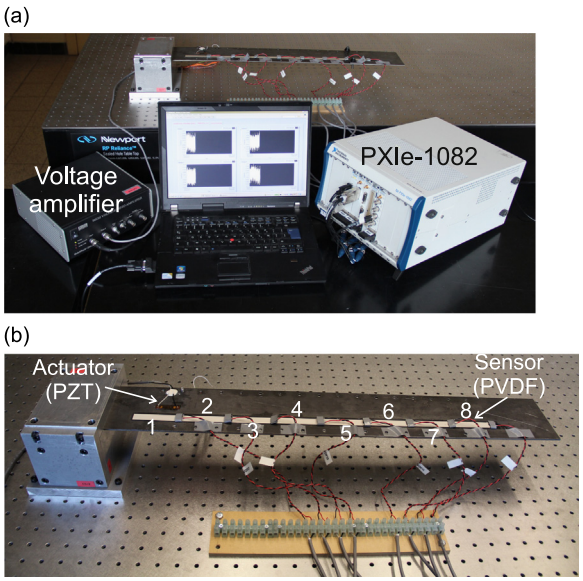

Fig. 13. Experimental setup. (a) Overall view, (b) clamped–free steel plate instrumented with 8 PVDF sensors.

Table 4
Durations of acquisition for the sampling frequencies tested.

f_s (Hz)	1600	3200	6400	12 800	25 600	51 200	102 400	204 800
T (s)	64	32	16	8	4	2	1	0.5

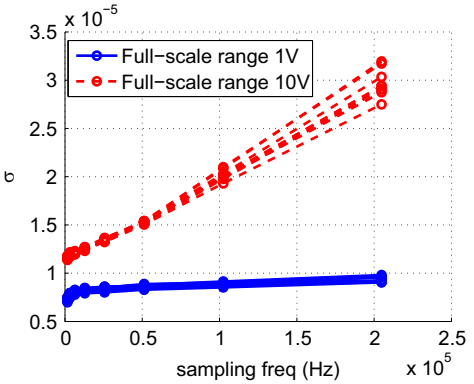

Fig. 14. Levels of noise for different sampling frequencies.

3.3. *Verification of noise of the sensors*

We have then investigated the noise on the sensors when (i) the sensors are connected to the acquisition system but not yet installed on the structure and (ii) when the sensors are installed on the structure. Fig. 16 depicts a typical time history and its FFT for a sensor not yet fixed on the structure. In this test, all the sensors were lying on a foam installed on the antivibration table.

From these measurements it is very difficult to assess correctly the noise. Indeed, the time history shows that the signal is not steady, and its FFT reveals a non-negligible low frequency content due to the ground motion, despite the fact that the sensors were lying on a foam installed on the antivibration table. Other sources of vibration as observed in [39] can also explain these variations of time histories such as acoustic noise or operating machines in the laboratory. We can also observe sharp peaks at 50 Hz harmonics due to electrical interferences. The FFT is however quite flat in a large frequency bandwidth. This suggests some kind of normality in the noise, since a white noise has a constant frequency content.

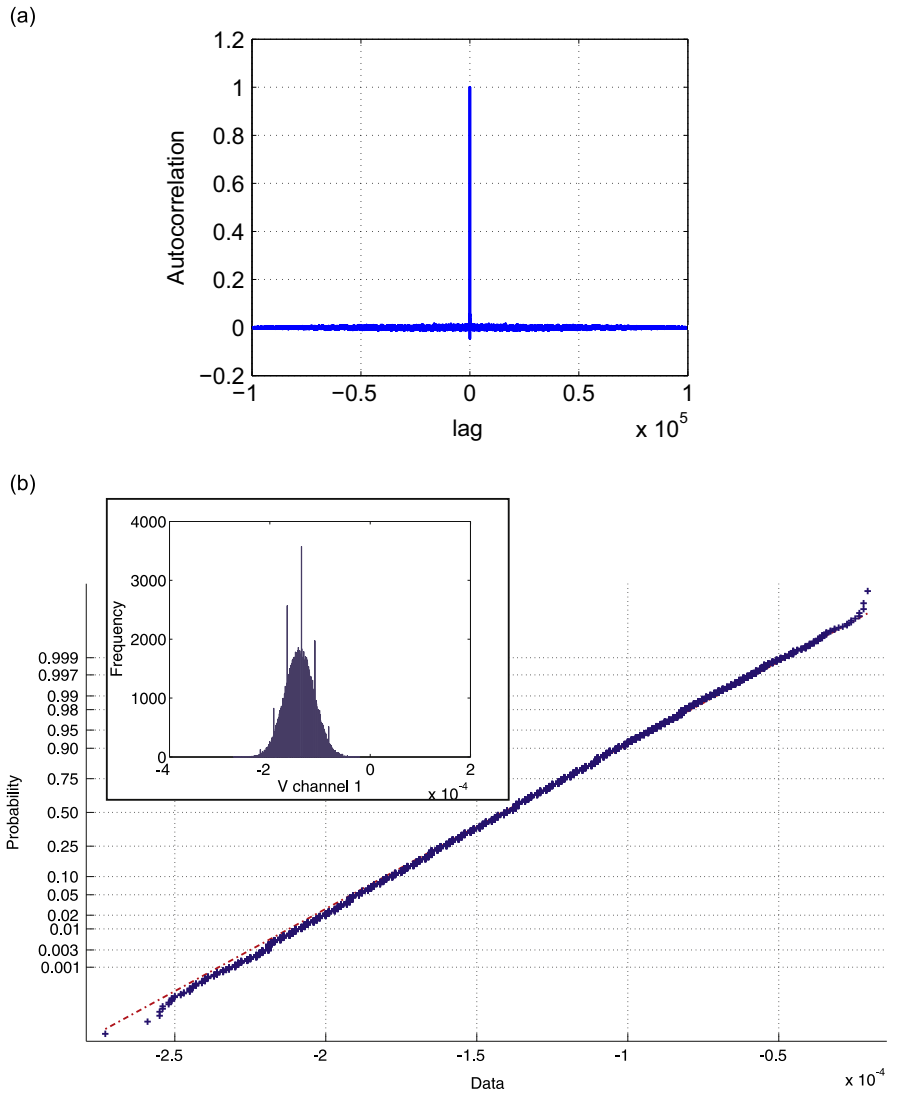

Fig. 15. Noise on channel 1 ($f_s = 204\,800$ Hz, full-scale range of 10 V). (a) Autocorrelation, (b) normal probability plot and histogram. Dashed line: normal distribution, crosses: sample data.

Fig. 17 gives an example of the time history and its FFT when the sensors have been fixed on the clamped–free setup, but with no forced excitation.

As for the sensors not fixed to the structure, the FFT is quite flat in a large frequency bandwidth and 50 Hz harmonics can be seen, but there are also other peaks. These peaks have been found to correspond to some eigenfrequencies of the clamped–free steel plate. For that reason, it was anew not possible to identify the noise, since most of the variability in the time history results from structural vibration and the 50 Hz harmonics. Fig. 18 illustrates the autocorrelation and the normal probability plot of the time history of Fig. 17.

Because of the 50 Hz harmonics and the structural vibration that has been discussed previously, there is a small correlation in the sensor response that can be observed, and the distribution does not follow a normal distribution since the data in the tails of the normal probability plot deviates from the straight line. Despite the fact that the results in the present section did not allow us to isolate the noise, we consider that the flat frequency content in a large frequency bandwidth that has been observed justifies the model of uncorrelated white noise proposed by Eq. (1).

3.4. Uncertainty on mode shapes

The clamped–free steel plate has been excited with the PZT patch shown in Fig. 13(b) with a band-limited white noise (flat PSD) between 0 Hz and 50 Hz exciting the two first bending mode shapes at 5.44 Hz and 33.07 Hz respectively, and the measurements last for 0.5 s with a sampling frequency of 51 200 Hz. In order to perform a statistical analysis of the

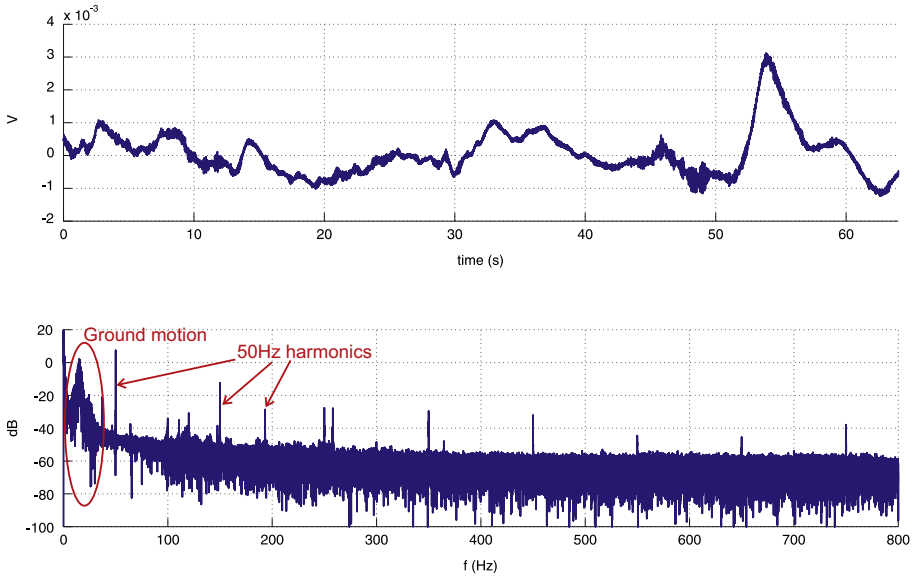

Fig. 16. Time history (top) and FFT (bottom) of sensor 1 lying on foam.

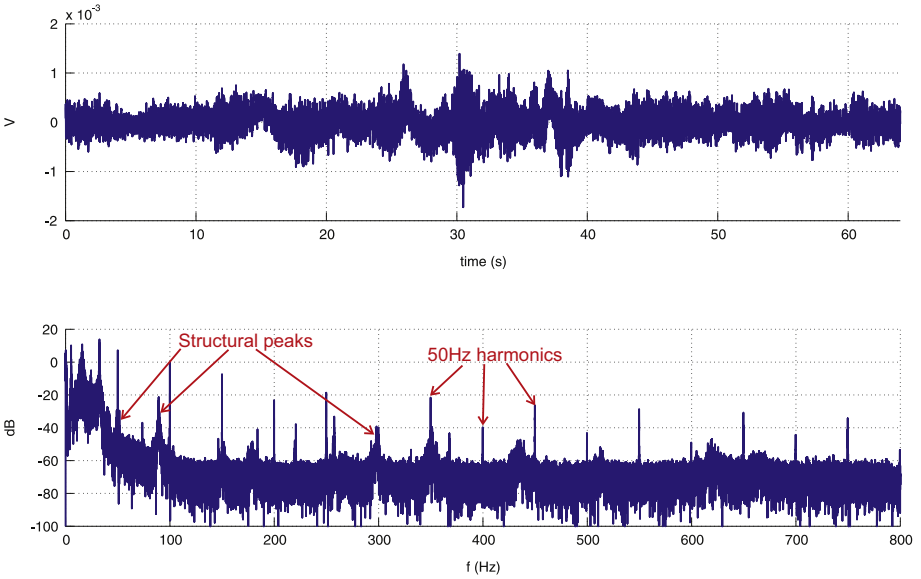

Fig. 17. Time history (top) and FFT (bottom) of sensor 1 fixed on the clamped–free setup (ambient vibration).

uncertainty on modal parameters due to noise measurement, a set of 4000 measurements has been collected, from which the modal parameters (mode shapes, eigenfrequencies and modal damping coefficients) have been identified with the *Macec* toolbox under *Matlab* as in the numerical case study. All the measurements have been acquired in a row within 12 h, during which no major environmental changes have been observed as discussed in Section 3.5. Fig. 19 shows a typical stabilization diagram obtained with the experimental case study. In this experiment, all the samples of the first mode shape have been obtained with a model order of 32, while all the samples of the second mode shape have been obtained with a model order of 28.

Similar to the numerical study, a pre-processing based on Eq. (10) to remove the wrong identifications of mode shapes from the baseline has been applied. Table 5 summarizes the success rates of the modal identifications for the first two bending mode shapes of the clamped–free steel plate.

It can be seen that the success ratio of modal identification is very good since maximum 6.3 percent of the modal identifications failed, but is much smaller than the numerical case study, for which maximum 0.04 percent of the modal identifications failed (see Table 1). Fig. 20 shows the mean of the identified mode shapes, as well as the 3σ variability intervals.

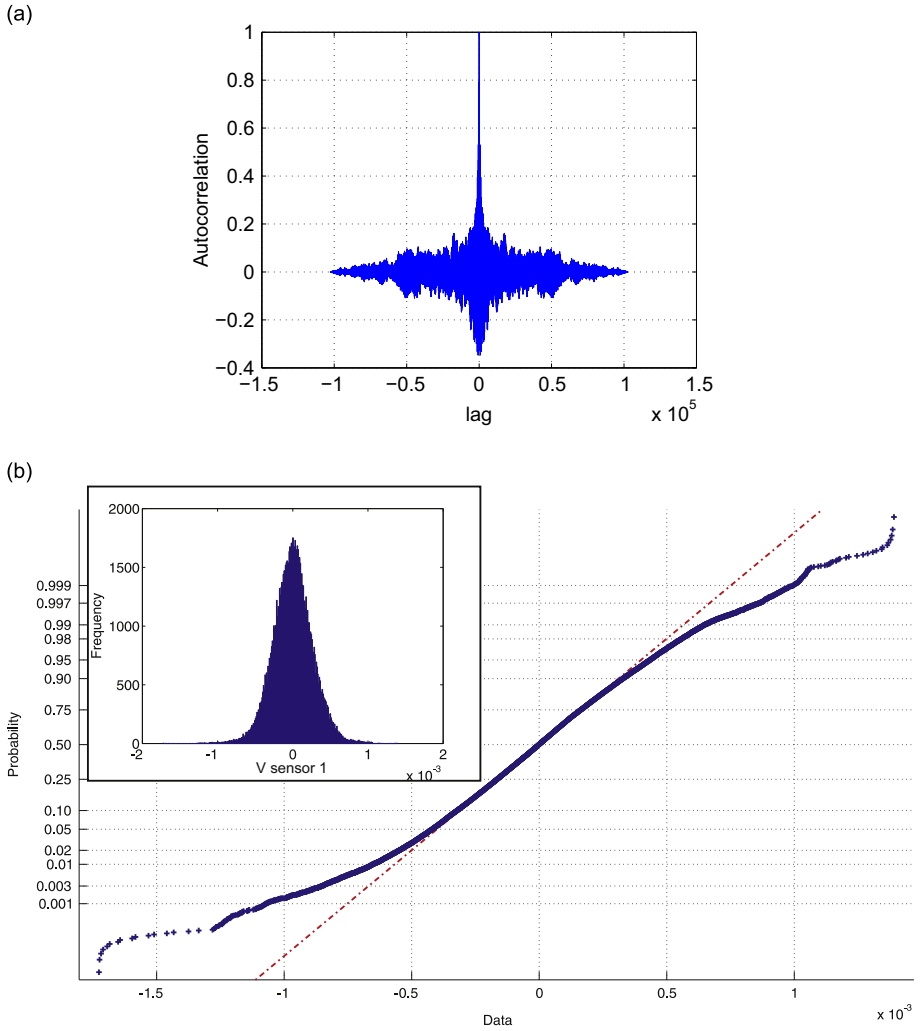

Fig. 18. Noise on sensor 1 ($f_s = 1600$ Hz, full-scale range of 1 V) under ambient excitation. (a) Autocorrelation, (b) normal probability plot and histogram. Dashed line: normal distribution, crosses: sample data.

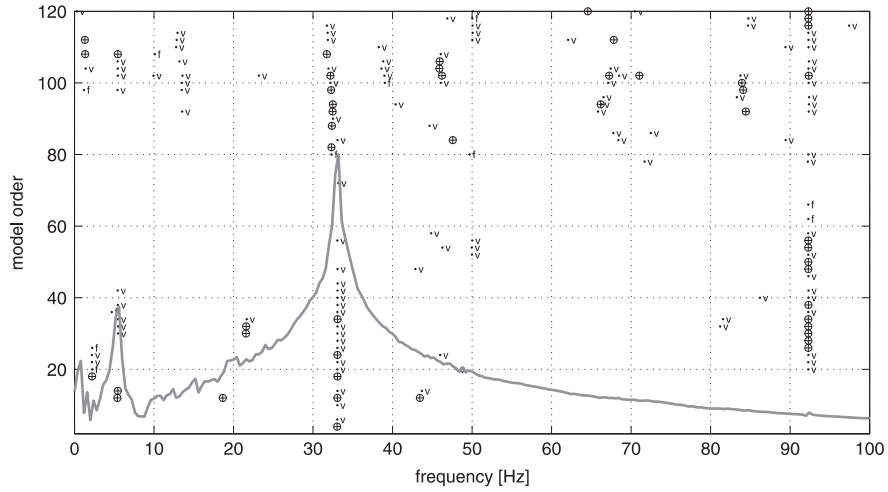

Fig. 19. Stabilization diagram obtained with one sample of the experimental case study (the grey thick curve represents the sum of PSDs of all sensors).

Table 5
Success rates of modal identifications.

Success quantifier	Φ_1	Φ_2
Number of samples retained N	3748	3985
Proportion of failed identification (%)	6.3	0.38

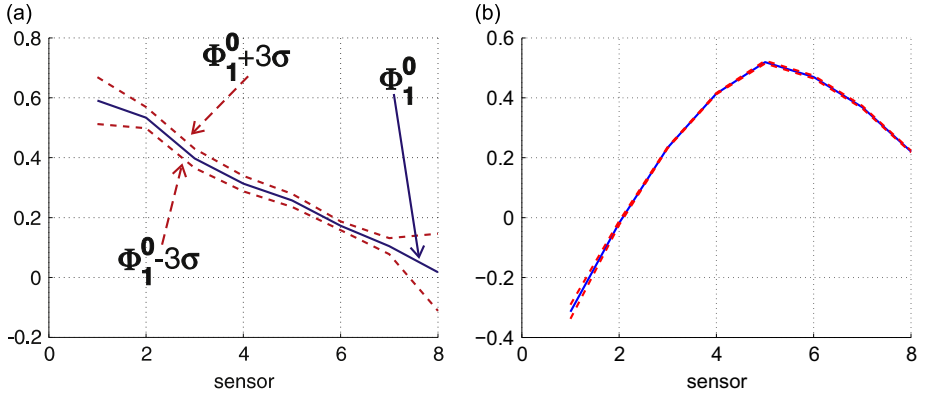

Fig. 20. Strain mode shapes of interest. Full line: strain mode shape (mean over all the samples), dashed line: 3σ interval. (a) Φ_1, (b) Φ_2.

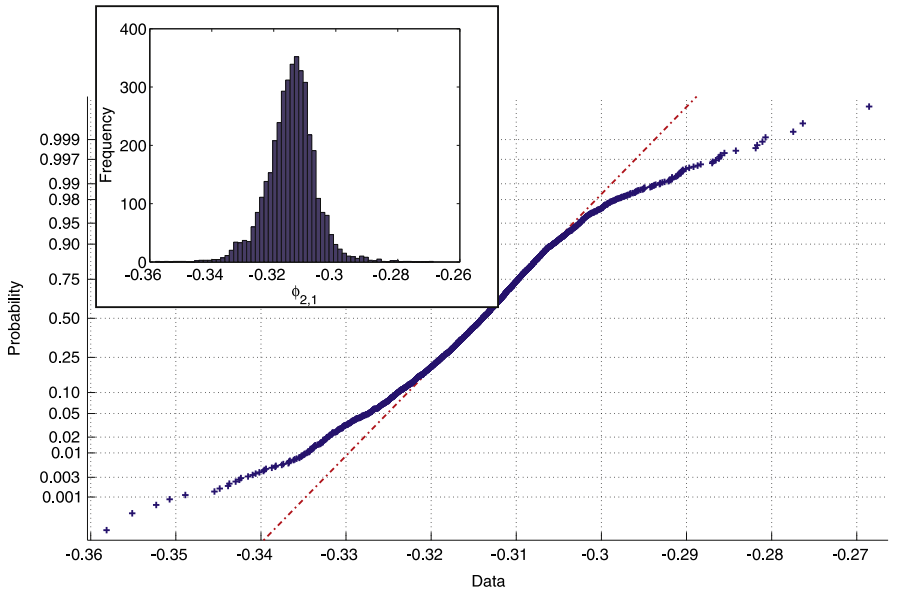

Fig. 21. Normal probability plot and histogram for the first component of Φ_2. Dashed line: normal distribution, crosses: sample data.

It can be observed that the uncertainty on the strain mode shapes (i.e. the 3σ interval) is bigger with the first bending mode shape, which explains why more samples of the first bending mode shape were rejected. Moreover, this observation shows that considering the same level of uncertainty for all the mode shapes is wrong. Indeed, depending on the excitation, the mode shapes will be more or less excited and therefore more or less easy to identify. It is also worth mentioning that while the noise on the channels was shown to be Gaussian, the hypothesis of a Gaussian distribution of the mode shape component at each sensor is less satisfying, as it can be seen from Fig. 21. Indeed, significant departure from the straight line is observed. This observation shows that the idea according to which the effect on the identified mode shape of an uncorrelated white noise on measurements can be modeled with a white noise on each component is not exact.

As with the numerical case study, we checked the convergence of the correlation matrices based on the NMD for each column of the correlation matrix when it is computed with n_s and n_s-50 samples. Fig. 22 shows the evolution of the NDM

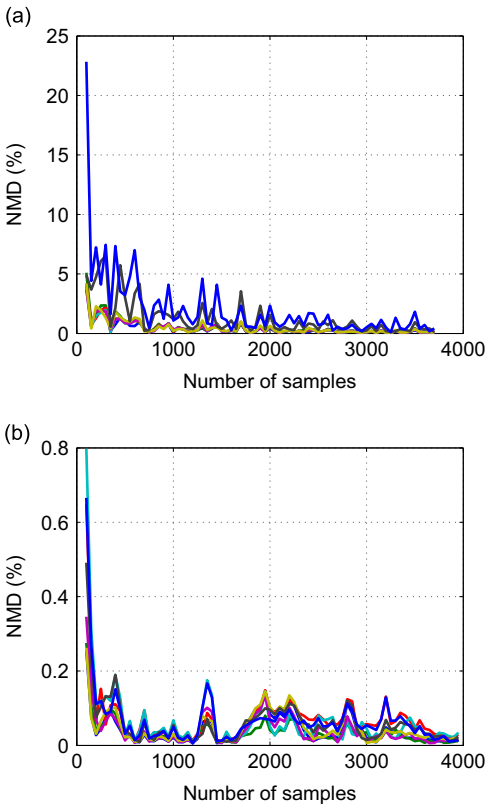

Fig. 22. Convergence of the correlation matrix based on the NMD value. (a) Φ_1, (b) Φ_2.

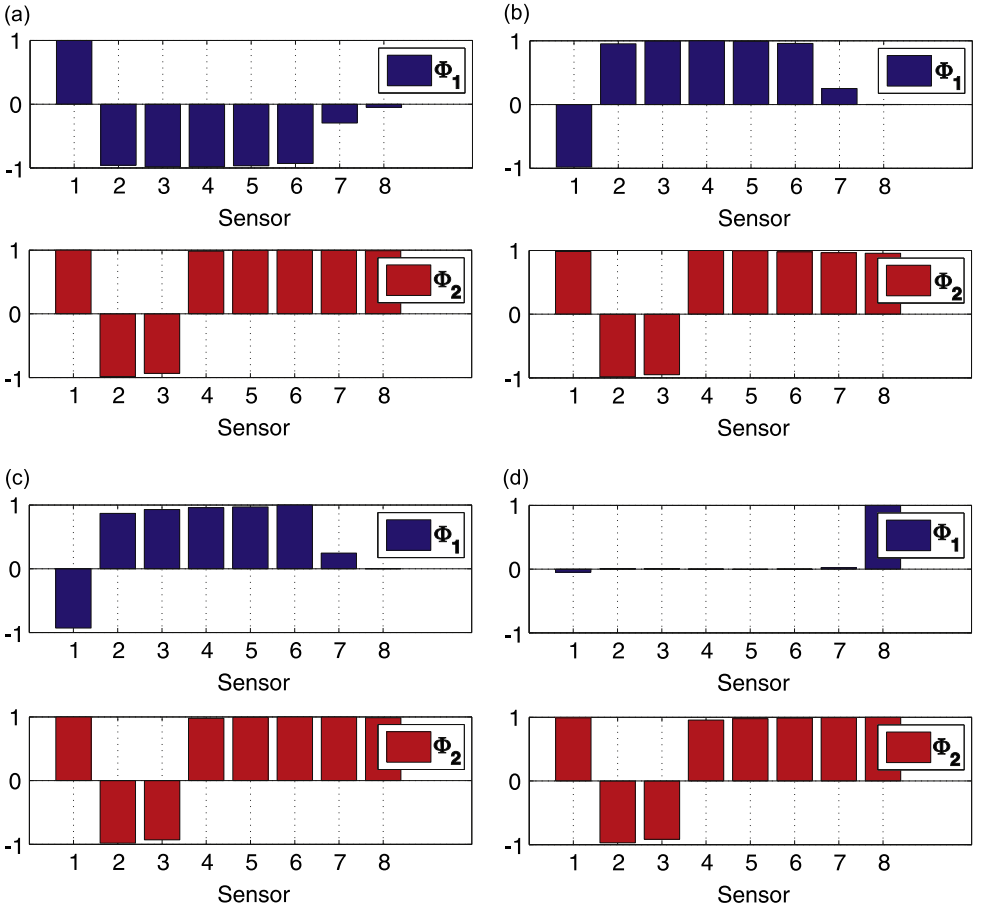

Fig. 23. Correlation coefficients. (a) Sensor 1, (b) Sensor 4, (c) Sensor 6, (d) Sensor 8.

value computed for all the columns of the correlation matrices of modes $\boldsymbol{\Phi}_1$ and $\boldsymbol{\Phi}_2$. It can be seen that the correlation matrices calculated with 3748 and 3985 samples for the first and the second bending mode shapes respectively can be considered as converged, since the NMD value stays below 2 percent for the first mode shape and 0.2 percent for the second one.

The analysis of Fig. 23 confirms the numerical predictions obtained in Section 2: the uncertainties at the different sensors are strongly spatially correlated. Indeed, there are many correlation coefficients $c_{i,mn}$ close to ± 1 for $m \neq n$.

Similar to the numerical case study, we then perform a singular value decomposition to illustrate the energy distribution in an independent variables space. Fig. 24 illustrates the singular values of the correlation matrices for modes $\boldsymbol{\Phi}_1$ and $\boldsymbol{\Phi}_2$.

Fig. 24 shows that the energy is contained in only a very few singular values, and confirms the properties observed previously in the numerical study. The uncertainty on the first mode shape is mainly explained by 3 eigenvectors, while only one eigenvector allows us to characterize most of the uncertainty on the second mode shape. Figs. 25 and 26 compare the first, fourth and eighth eigenvectors of the correlation matrices for modes 1 and 2 respectively. We see that the principal eigenvector $\mathbf{u}_1$ is quite similar to the correlation coefficients of the first columns for $\boldsymbol{\Phi}_1$ with an opposite sign (see Fig. 23(a), (b) and (c)), while the first eigenvector for $\boldsymbol{\Phi}_2$ is almost identical (again with an opposite sign) to all the columns of the correlation matrix (see Fig. 23), since there is only one main singular value.

3.5. Uncertainty on eigenfrequencies and modal damping coefficients

Tables 6 and 7 summarize the mean values and the corresponding standard deviations of each eigenfrequency and modal damping coefficient. In particular, a huge uncertainty on the modal damping coefficients can be observed.

It is worth mentioning that the uncertainty on f_1 and ξ_1 is bigger than on f_2 and ξ_2. Similarly, the uncertainty on $\boldsymbol{\Phi}_1$ is bigger than on $\boldsymbol{\Phi}_2$ as illustrated in Fig. 20. This observation can be explained by the fact that the second mode shape is more excited than the first one as it can be seen on the stabilization diagram of Fig. 19: the sum of PSDs (grey curve) has a much higher peak at the second eigenfrequency than at the first one. Also, the very short acquisition time (0.5 s) makes the identification of low frequency mode shapes less accurate. It is therefore more difficult to identify the modal parameters of

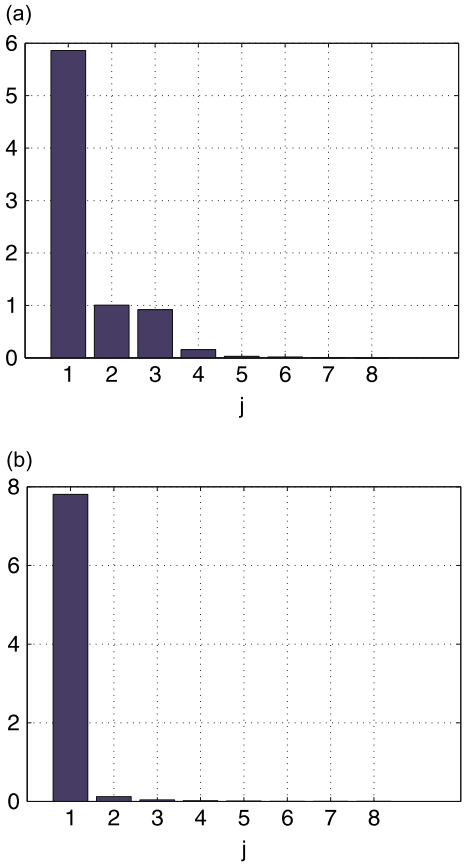

Fig. 24. Singular values of the correlation matrices. (a) $\boldsymbol{\Phi}_1$, (b) $\boldsymbol{\Phi}_2$.

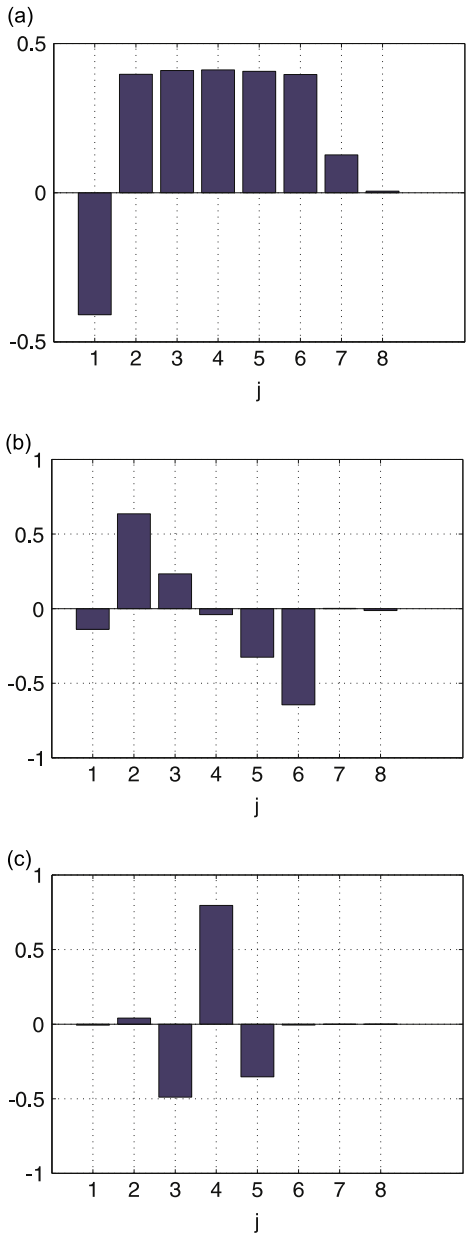

Fig. 25. Eigenvectors of the correlation matrix of $\mathbf{\Phi}_1$. (a) $\mathbf{u}_1$, (b) $\mathbf{u}_4$, (c) $\mathbf{u}_8$.

the first mode shape than the second one (Table 5 shows that there are more identifications which failed for the first mode shape). Consequently, there is more uncertainty on the modal parameters of the first mode shape.

The normal probability plots of Figs. 27 and 28 confirm also the non-Gaussian nature of the uncertainties on the identified eigenfrequencies and modal damping coefficients that was previously observed with the numerical investigation. In fact, the histograms of Fig. 28 suggest that the modal damping coefficients follow a lognormal distribution, despite the fact that there are some identified values of ξ_1 and ξ_2 that are negative, but such modal damping coefficients are not physical. The damping coefficients of lightly damped modes estimated with the stochastic subspace identification can have a nonzero probability at negative values because the identified system description is not restricted to be stable.

Since it is well known that environmental changes such as changes of temperature can strongly affect the eigenfrequencies [40,41], it is important to verify whether the non-Gaussian distribution is due to any environmental changes. For this purpose, we display in Fig. 29 the chronological evolution of identified eigenfrequencies. It is very clear that the eigenfrequencies are steady and do not follow any trend. This shows that the non-Gaussian distribution of the identified eigenfrequencies does not come from any environmental effects, but is a property of the uncertainty on modal parameters estimated with the stochastic subspace method.

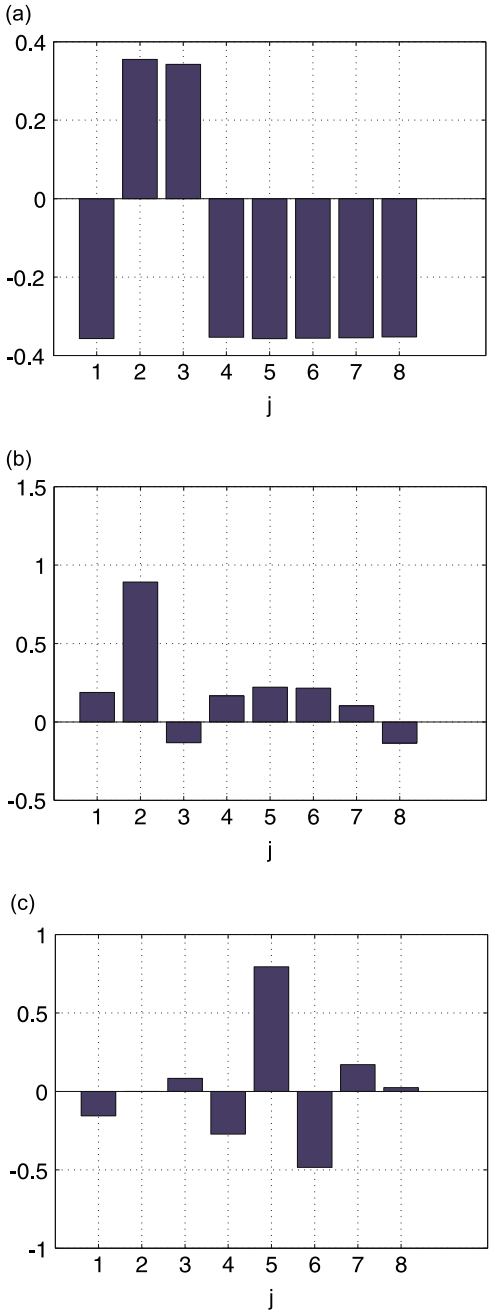

Fig. 26. Eigenvectors of the correlation matrix of $\mathbf{\Phi}_2$. (a) $\mathbf{u}_1$, (b) $\mathbf{u}_4$, (c) $\mathbf{u}_8$.

Table 6
Uncertainties on the identified eigenfrequencies.

	μ (Hz)	σ (%)
f_1	5.44	1.51
f_2	33.07	0.01

The non-correlation between modal parameters that was obtained with the numerical case study (see Fig. 11) has also been observed with the experimentally identified eigenfrequencies and modal damping coefficients, as illustrated in Fig. 30.

Table 7
Uncertainties on the identified modal damping.

	μ (%)	σ (%)
ξ_1	1.09	1.55
ξ_2	0.20	0.66

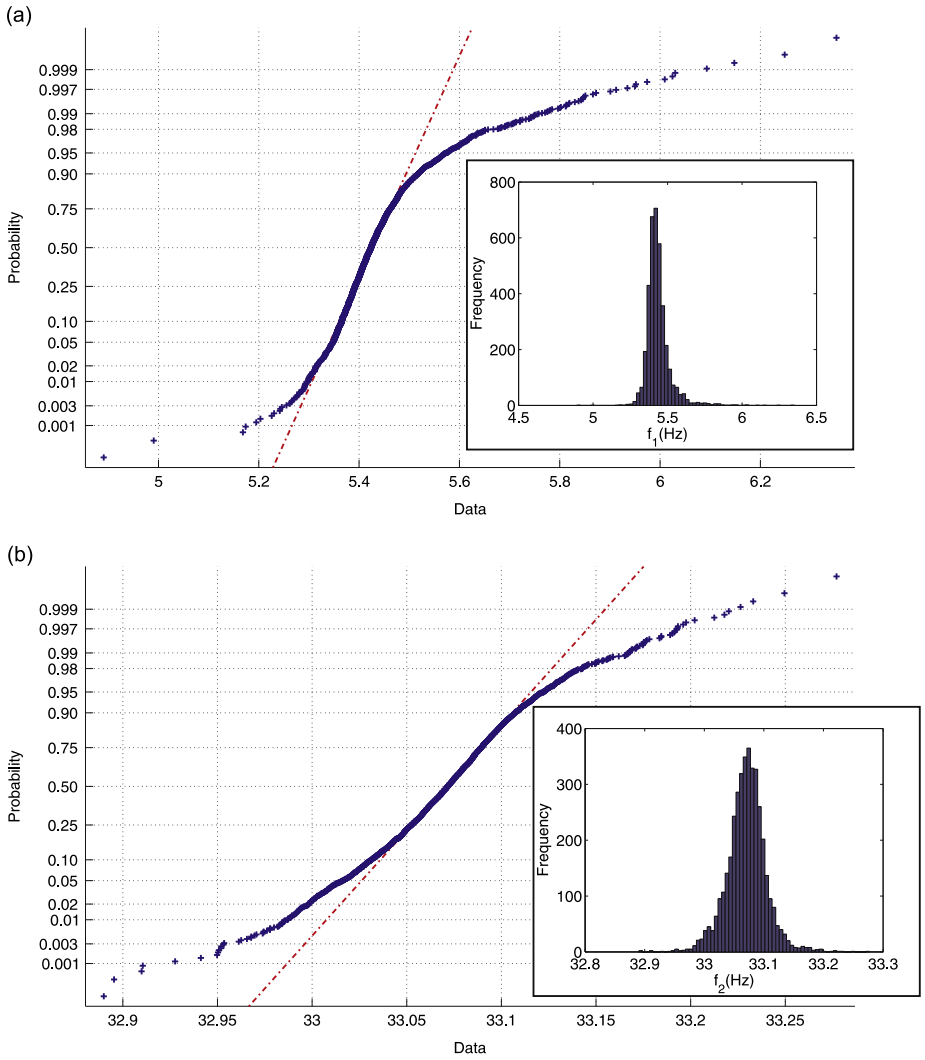

Fig. 27. Normal probability plots and histograms of the eigenfrequencies. Dashed line: normal distribution, crosses: sample data. (a) f_1, (b) f_2.

4. Conclusion

In this paper, we have studied the effect of noise measurement on the uncertainty of modal parameters identified using stochastic subspace identification. A first numerical investigation deals with a simply supported beam, and 5000 modal identifications have been performed in a Monte-Carlo simulation to estimate the uncertainty on modal parameters when the noise is added on the sensors before modal analysis under the form of uncorrelated white noise. A comparison of the results obtained from this Monte-Carlo simulation with the common approach which consists in adding uncorrelated white noise on the modal parameters directly to model the effect of noise measurement pointed out that the uncertainty on modal parameters might exhibit a non-normal distribution. We have also illustrated by computing the correlation matrices that the modal identification introduces some spatial correlation in the noise between the sensors, so that adding spatially uncorrelated white noise on the mode shapes is not correct. These observations have been then verified experimentally

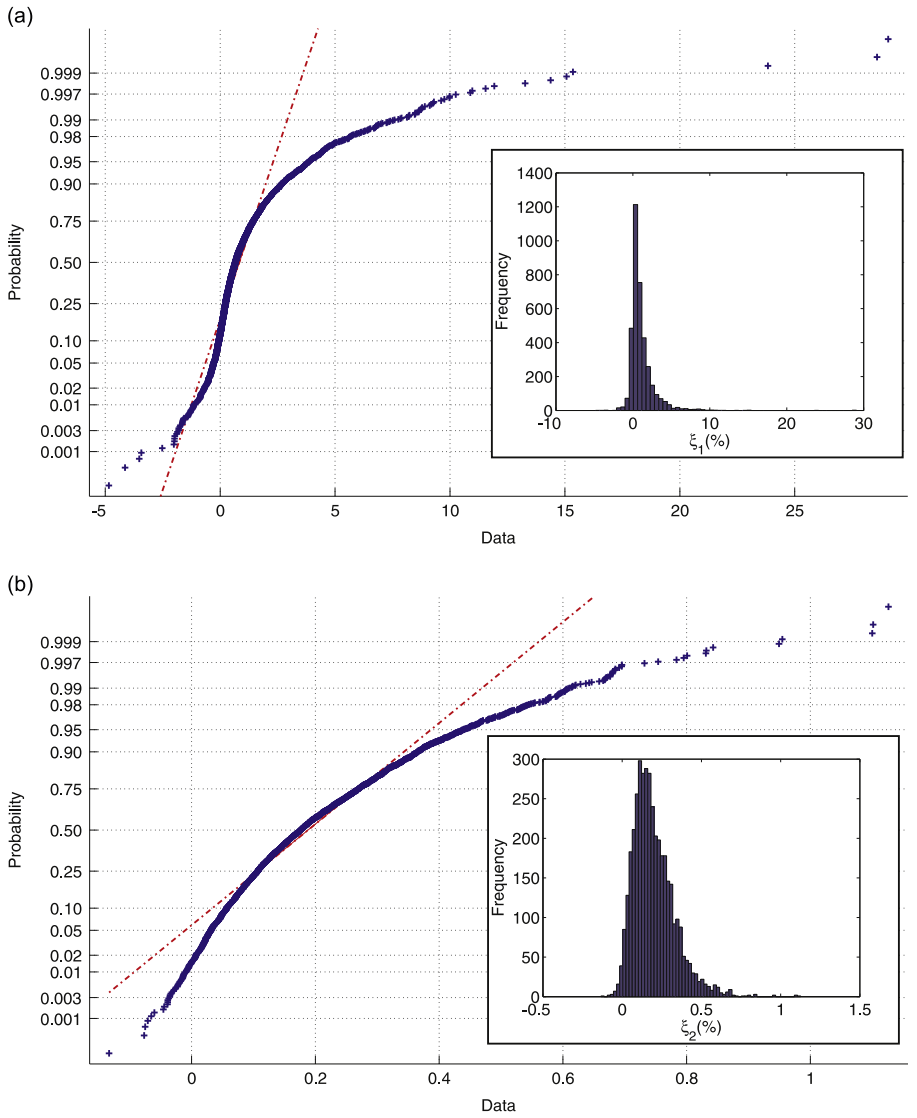

Fig. 28. Normal probability plots and histograms of the modal damping coefficients. Dashed line: normal distribution, crosses: sample data. (a) ξ_1, (b) ξ_2.

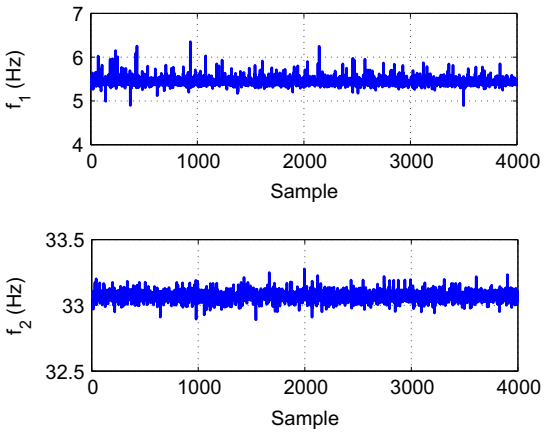

Fig. 29. Evolution of the identified eigenfrequencies in chronological order.

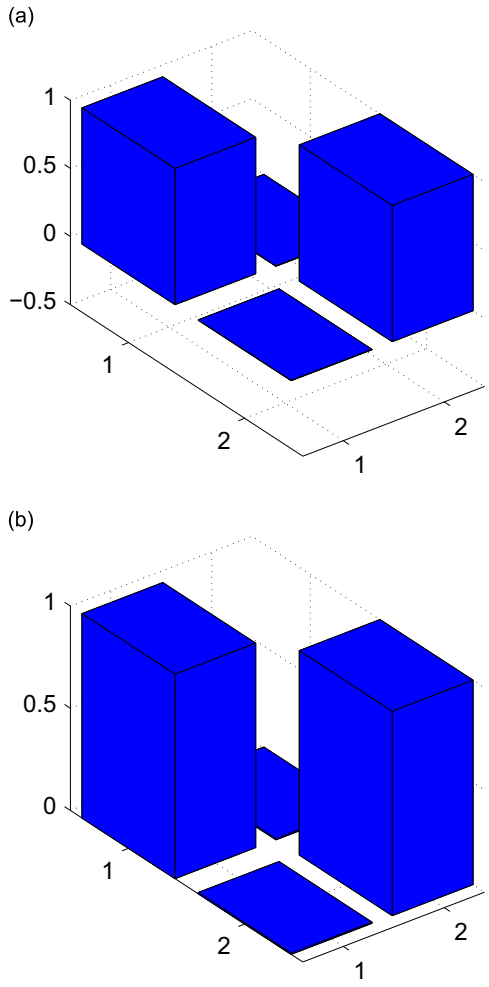

Fig. 30. Correlation of the uncertainty on the modal parameters. (a) Eigenfrequencies, (b) modal damping coefficients.

with a small clamped–free steel plate instrumented with 8 piezoelectric patches, and actuated with a piezoceramic patch. After characterizing the noise of the data acquisition system, 4000 modal identifications of the two first bending mode shapes have been performed, and the correlation matrices have been computed, confirming the spatial correlation between the noise on the sensors as numerically pointed out. In addition, a non-normal distribution is also observed for the first two eigenfrequencies and the corresponding modal damping coefficients. This study suggests that caution should be taken when assuming noise models directly on identified modal parameters. It is important to note that the findings of this work are only valid for the stochastic subspace method, for which it was not possible to propose a noise model to be applied directly on the modal parameters. Also, all the results discussed in this study have been obtained for specific model orders. More investigations are needed to check out if these results depend on the choice of model order. Although expensive in computation, it is advised to identify noise models based on time domain simulations in which the noise is directly added on the time domain sensor responses. As these models will be specific to each structure as well as the modal identification method used, it requires to perform costly computations but ensures much more realistic representation of the effect of noise on the modal parameters.

Acknowledgments

The first author has been supported by a F.R.I.A (grant no. FC86240) from the F.N.R-F.N.R.S of Belgium, while the second author is a Research Associate of the F.N.R-F.N.R.S. The authors would like to thank Gilles Vanhooren for manufacturing the experimental setups and Dr. Edwin Reynders of KU Leuven for very helpful discussions on stochastic subspace identification.

References

[1] E. Reynders, G. De Roeck, Reference-based combined deterministic–stochastic subspace identification for experimental and operational modal analysis, *Mechanical Systems and Signal Processing* 22 (2008) 617–637.
[2] E. Reynders, M. Schevenels, G. De Roeck, MACEC 3.1: a Matlab toolbox for experimental and operational modal analysis, Report BWM-2010-05, Department of Civil Engineering, K.U. Leuven, 2010.
[3] M.I. Friswell, J.E. Mottershead, *Finite Element Model Updating in Structural Dynamics*, Kluwer Academic Publishers, London, 1999.
[4] E. Reynders, G. De Roeck, Damage identification on the Tilff bridge by vibration monitoring using finite element model updating, *Proceedings of Experimental Vibration Analysis for Civil Engineering Structures*, Bordeaux, France, 2005.
[5] A. Teughels, Inverse Modelling of Civil Engineering Structures Based on Operational Modal Data, PhD Thesis, Department of Civil Engineering, Katholieke Universiteit Leuven, 2003.
[6] S.W. Doebling, C.R. Farrar, M.B. Prime, D.W. Shevitz, Damage identification and health monitoring of structural and mechanical systems from changes in their vibration characteristics: a literature review, Los Alamos National Laboratory Report LA-13070-MS, 1996.
[7] A. Raghavan, C.E.S. Cesnik, Review of guided-wave structural health monitoring, *Journal of Vibration and Acoustics* 39 (2007) 91–114.
[8] G.E.P. Box, G.M. Jenkins, G.C. Reinsel, *Time Series Analysis: Forecasting and Control*, Prentice-Hall, New Jersey, 1994.
[9] H. Sohn, C.R. Farrar, Damage diagnosis using time series analysis of vibration signals, *Smart Materials and Structures* 10 (2001) 446–451.
[10] K.K. Nair, A.S. Kiremidjian, K.H. Law, Time series-based damage detection and localization algorithm with the application to the ASCE benchmark structure, *Journal of Sound and Vibration* 291 (2006) 349–368.
[11] O.D. Salawu, Detection of structural damage through changes in frequency: *a review*, *Engineering Structures* 19 (1997) 718–723.
[12] K.L. Napolitano, J.B. Kosmatka, Damage detection of highly damped structures using direct frequency response measurements and residual force vectors, *Proceedings of SPIE Smart Structures and Materials*, San Diego CA, USA, 1996.
[13] S. Alampalli, Effects of testing, analysis, damage and environment on modal parameters, *Mechanical Systems and Signal Processing* 14 (2000) 63–74.
[14] A.K. Pandey, M. Biswas, M.M. Samman, Damage detection from changes in curvature mode shapes, *Journal of Sound and Vibration* 145 (1991) 321–332.
[15] A.K. Pandey, M. Biswas, Damage detection in structures using changes in flexibility, *Journal of Sound and Vibration* 169 (1994) 3–17.
[16] N. Stubbs, J.Y. Kim, Damage localization in structures without baseline modal parameters, *American Institute of Aeronautics and Astronautics Journal* 34 (1996) 1644–1649.
[17] P. Cornwell, S.W. Doebling, C. Farrar, Application of strain energy damage detection method to plate-like structures, *Journal of Sound and Vibration* 224 (1999) 359–374.
[18] E. Reynders, R. Pintelon, G. De Roeck, Uncertainty bounds on modal parameters obtained from stochastic subspace identification, *Mechanical Systems and Signal Processing* 22 (2007) 948–969.
[19] D. Wu, S.S. Law, Damage localization in plate structures from uniform load surface curvature, *Journal of Sound and Vibration* 276 (2004) 227–244.
[20] A. Philips Adewuyi, Z. Wu, N.H.M. Kammrujaman Serker, Assessment of vibration-based damaged identification methods using displacement and distributed strain measurements, *Journal of Structural Health Monitoring* 8 (2009) 443–461.
[21] H. Guan, V.P. Karbhari, Improved damage detection method based on element modal strain damage index using sparse measurements, *Journal of Sound and Vibration* 309 (2008) 465–494.
[22] A.M. Yan, G. Kerschen, P. De Boe, J.C. Golinval, Structural damage diagnosis under varying environmental conditions—Part I: *a linear analysis*, *Mechanical Systems and Signal Processing* 19 (2005) 847–864.
[23] Z. Wang, K.C.G. Ong, Structural damage detection using autoregressive-model-incorporating multivariate exponentially weighted moving average control chart, *Journal of Engineering Structures* 31 (2009) 1265–1275.
[24] U. Galvanetto, G. Violaris, Numerical investigation of a new damage detection method based on proper orthogonal decomposition, *Journal of Mechanical Systems and Signal Processing* 21 (2007) 1246–1261.
[25] R. Pintelon, P. Guillaume, J. Schoukens, Uncertainty calculation in (operational) modal analysis, *Mechanical Systems and Signal Processing* 21 (2007) 2359–2373.
[26] M. Dohler, L. Mevel, Efficient multi-order uncertainty computation for stochastic subspace identification, *Mechanical Systems and Signal Processing* 38 (2013) 346–366.
[27] E. Carden, A. Mita, Challenges in developing confidence intervals on modal parameters estimated for large civil infrastructure with stochastic subspace identification, *Structural Control Health Monitoring* 18 (2011) 53–78.
[28] G. Tondreau, E. Reynders, A. Deraemaeker, Towards a more realistic modeling of the uncertainty on identified mode shapes due to measurement noise, *Proceedings of the Ninth International Conference on Damage Assessment of Structures*, Oxford, UK, 2011.
[29] SDTools, Structural Dynamic Toolbox ⟨http://www.sdtools.com⟩ (Accessed 22 July 2013).
[30] A. Preumont, Frequency domain analysis of time integration operators, *Earthquake Engineering and Structural Dynamics* 10 (1982) 691–697.
[31] G. Tondreau, A. Deraemaeker, Local modal filters for automated data-based damage localization using ambient vibrations, *Mechanical Systems and Signal Processing* 39 (2013) 162–180.
[32] A.V. Oppenheim, R.W. Schafer, J.R. Buck, *Discrete-time Signal Processing*, Prentice-Hall, New Jersey, 1999.
[33] P. Van Overschee, B. De Moor, *Subspace Identification for Linear Systems: Theory and Implementation—Application*, Kluwer Academic Publishers, Dordrecht, Netherlands, 1996.
[34] B. Peeters, G. De Roeck, Reference-based stochastic subspace identification for output-only modal analysis, *Mechanical Systems and Signal Processing* 13 (1999) 855–878.
[35] D.J. Ewins, *Modal Testing: Theory and Practice*, Research Studies Press Ltd, Letchworth, 1984.
[36] T.P. Ryan, *Statistical Methods for Quality Improvement*, John Wiley and Sons, New York, 2000.
[37] D.C. Montgomery, *Statistical Quality Control: A Modern Introduction*, John Wiley and Sons, New York, 2009.
[38] G. Tondreau, A. Deraemaeker, Experimental localization of small damages using modal filters, *Proceedings of IMAC XXXI*, Garden Grove CA, USA, February 2013.
[39] M. Boudaoud, Y. Haddab, Y. Le Gorrec, P. Lutz, Noise characterization in millimeter sized micromanipulation systems, *Mechatronics* 21 (2011) 1087–1097.
[40] B. Peeters, G.D. Roeck, One-year monitoring of the Z24-Bridge: *environmental effects versus damage events*, *Earthquake Engineering and Structural Dynamics* 30 (2001) 149–171.
[41] H. Sohn, M. Dzwonczyk, E.G. Straser, A.S. Kiremidjian, K.H. Law, T. Meng, An experimental study of temperature effect on modal parameters of Alamosa canyon bridge, *Earthquake Engineering and Structural Dynamics* 28 (1999) 879–897.